Title

An electrostatic finite element analysis of the electrospinning process of bilayer constructs using a parallel-plate collector

Authors

Molina, Maria I Echeverria
Komvopoulos, Kyriakos

Publication Date

2022-04-01

DOI

10.1016/j.matlet.2022.131649

Peer reviewed

Materials Letters 313 (2022) 131649

Contents lists available at ScienceDirect

Materials Letters

journal homepage: www.elsevier.com/locate/matlet

An electrostatic finite element analysis of the electrospinning process of bilayer constructs using a parallel-plate collector

Maria I. Echeverria Molina, Kyriakos Komvopoulos *

Department of Mechanical Engineering, University of California, Berkeley, CA 94720, USA

ARTICLE INFO

Keywords:
Electric potential
Electrospinning
Fiber orientation
Finite element analysis
Morphology
Simulation

ABSTRACT

Fundamental knowledge of the deposition process of electrospun fibers is of paramount importance to the fabrication of constructs with fibers oriented in specific directions, depending on the mandrel geometry. This paper presents an electrostatic finite element analysis of a parallel-plate electrospinning configuration that reveals the effects of the electric potential intensity and directionality on the deposition of aligned and randomly oriented fibers, resulting in the formation of a fibrous bilayer construct. Simulations demonstrate that polymer deposition between the collector plates yields a local effect on the electric field. This study provides a computational methodology for investigating other collector configurations and guidance for designing electrospinning setups capable of producing microfibrous constructs with tailored morphologies.

1. Introduction

Electrospinning is a conventional yet versatile manufacturing process for fabricating fibrous constructs and scaffolds for multiple applications, including aerosol particle filtration, proton exchange membranes for fuel cells, and scaffolds for tissue engineering [1–3]. Basic knowledge of the electrospinning process is critical because it controls the morphology and physical attributes of the fabricated construct. Specifically, the internal structure and biomechanical properties of electrospun scaffolds strongly depend on the fiber diameter and alignment, porosity, and pore size, which affect the mechanical performance of the scaffold and its affinity to elicit a specific cellular behavior [4,5]. Cell alignment along the fiber orientation, cell infiltration, cell migration to specific directions, and cell differentiation are characteristic examples of the effect of a fibrous scaffold morphology that mimics the extracellular matrix of tissues like cartilage, neural tissue, and bone [4]. Therefore, the design of an electrospinning setup that can produce constructs with desired morphologies is of paramount importance. For instance, bilayer constructs consisting of aligned and randomly oriented fibers fabricated with a parallel-plate collector demonstrated enhanced cell proliferation and migration [6].

Although fibrous constructs possessing various morphologies have been fabricated with different collector designs [7,8], knowledge of the effect of the mandrel configuration on the electric field of the deposition process is mostly empirical. Previous simulations have provided insight into the overall electric field intensity but not the directionality [9,10]. Therefore, a comprehensive analysis of the electric field produced by a specific mandrel geometry is essential to understand the physical aspects of the electrospinning process and accordingly guide the design of systems that can produce constructs with versatile fibrous architectures.

The finite element analysis (FEA) is a powerful method for performing electrostatic simulations of the electrospinning process, which can illuminate the effects of the directionality and intensity of the electric field on the construct morphology. Consequently, the objective of this study was to perform FEA simulations of the electrostatic field of the electrospinning process for a parallel-plate collector configuration, used to fabricate bilayer constructs with aligned and randomly oriented fibers [7]. The thickness effect of polymer deposited between the collector plates on the electric field in the vicinities of the needle tip and the plates and the variation of the electric field intensity with the distance from the needle tip, the plate edge, and along the symmetry plane of the electrospinning system are interpreted in the context of FEA results. The simulations provide explanation for the fiber alignment between the plates, and the deposition of randomly oriented fibers beyond a critical polymer thickness due to the diminishing directionality of the electric field.

2. Simulation methodology

The electrostatic analysis of the parallel-plate electrospinning system

* Corresponding author.
E-mail address: kyriakos@me.berkeley.edu (K. Komvopoulos).

https://doi.org/10.1016/j.matlet.2022.131649
Received 6 October 2021; Received in revised form 19 December 2021; Accepted 2 January 2022
Available online 6 January 2022

was performed with the FEA software COMSOL Multiphysics (version 5.6), using the electrostatics module. The setup includes an aluminum mandrel consisting of a 27-mm-diameter shaft insulated with a 10-mm-thick polydimethylsiloxane layer of 2.6 relative permittivity and two parallel plates of 58 mm diameter, 5 mm thickness, and 15 mm distance from each other, a steel needle, and an aluminum holder of the needle. The distance between the needle tip and the shaft axis was kept constant at 120 mm, as in the experiments. The surrounding medium is air. A poly-L-lactic acid (PLLA) layer of 3.51 relative permittivity [11] and thickness up to 300 μm is modeled between the plates, with its bottom surface located 100 μm below the inner edge of the plates. The entire electrospinning setup is enclosed in a simulation box (1200 × 1000 × 600 mm^3). The foregoing simulation parameters are consistent with the experimental conditions used to fabricate bilayer scaffolds with a layer having fibers aligned between the plates and a layer with randomly oriented fibers. For uniform polymer coverage, the mandrel was rotated at 8.4 rpm. The electrospun solution consisted of 19% w/v of PLLA and hexafluoroisopropanol solvent. A flow rate of 1 ml/h was used in all the experiments.

The electrostatic analysis was performed for a potential of 14 kV applied to the needle holder and grounded collector, using Maxwell's equations and assuming insulated outer surface of the simulation box. The FEA mesh consisted of ~64,222,393 tetrahedral finite elements (depending on the polymer thickness) with a minimum size of 2 μm (Fig. 1a). To improve the accuracy, an algebraic multigrid preconditioned conjugate gradient solver was used at the expense of a longer computational time. Convergence studies confirmed that the results were not affected by the size of the simulation box. Introducing fillets to the inner edge of the plates and the edge of the needle tip decreased the electric field intensity only locally without affecting the observed trends. Accordingly, fillets were not used in the FEA model.

3. Results and discussion

The analyzed electrospinning system resembles a parallel-plate capacitor with the needle and its holder representing the plate to which the potential is applied and the grounded mandrel the other plate of the capacitor, with air or polymer plus air dielectric medium between the plates before and during electrospinning, respectively. Results are presented for the simplifying case of stationary mandrel and in tandem deposition between and at the top of the plates

Fig. 1b shows scanning electron microscopy (SEM) images of aligned and randomly oriented fibers of a bilayer construct fabricated with the aforementioned setup. These fiber morphologies are representative of all regions across the space between the plates. The electric field in the vicinities of the inner edge of the left plate and the needle tip for a 60-μm-thick polymer layer is shown in Fig. 1c(i) and 1c(ii), respectively. For comparison, the electric field adjacent to the plates and the needle tip for a 100-μm-thick polymer layer is shown in Fig. 1c(iii) and 1c(iv), respectively. While the electric field intensity decreases near the middle of the distance between the plates, it is still sufficiently strong and directional for aligning the fibers between the plates (Fig. 1b(i)). Although the deposited polymer does not affect the electric field at the needle tip, the increase of its thickness weakens the electric field at the top of the plates (Fig. 1c). Fig. 1d shows that the electric field intensity decreases abruptly with increasing distance from the needle tip up to ~5 mm, beyond which it decays fairly linearly at a very low rate. Similar results have been reported previously [9,10]. The localized sharp drop of the electric potential in the proximity of the grounded plates (inset of Fig. 1d) is due to the abrupt change in dielectric medium from air to polymer.

Fig. 2a shows the effect of polymer thickness on the variation of the electric field intensity with the *y*-distance (defined in the inset). The electric field intensity increases rapidly with the distance up to the polymer/air interface where a sharp drop is encountered. Importantly,

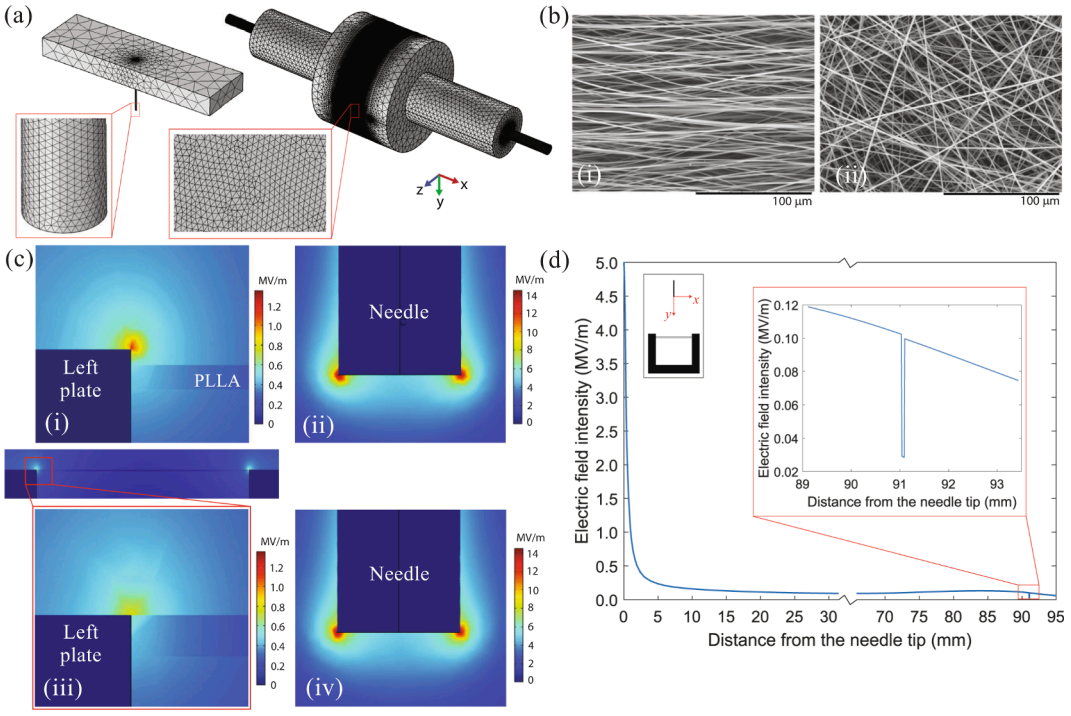

Fig. 1. (a) Finite element mesh of the needle holder (left) and mandrel assembly with a 60-μm-thick polymer layer between the plates (right). The models are not to scale. (b) SEM images of fiber morphologies representative of all the polymer regions between the plates of a bilayer construct consisting of (i) aligned and (ii) randomly oriented fibers. (c) Electric field intensity in the vicinities of (i) the left plate and (ii) the needle tip for a 60-μm-thick polymer layer, and (iii) between the plates and in the vicinities of the left plate and (iv) the needle tip for air dielectric. These plots were obtained at a plane dissecting the model along the needle axis and the mandrel axis. (d) Electric field intensity versus distance from the needle tip for a 60-μm-thick polymer layer. The distance from the needle tip is measured in the *y*-direction. The inset shows a cross-sectional view of the mandrel and the (*x*, *y*) coordinate system with its origin at the center of the needle tip.

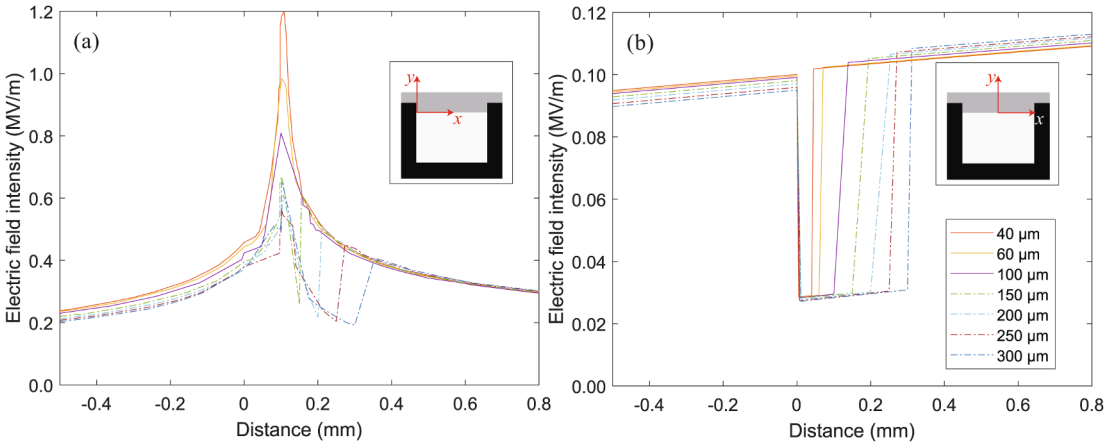

Fig. 2. Electric field intensity versus distance measured in the *y*-direction (specified in the insets) and polymer layer thickness (shown in the legend) along (a) the wall surface of the left plate and (b) the axisymmetric axis of the electrospinning system and the needle axis. The insets show cross-sectional views of the mandrel and the (*x*, *y*) coordinate system used in each plot. The origin of the coordinate system is 100 μm below the top of the plates and in (a) it is 5 μm to the right from the inner wall surface of the left plate, whereas in (b) it is in the middle of the distance between the plates.

the increase of the polymer layer thickness decreases the electric field intensity profoundly. A strengthened electric field arises in the vicinity of the plate edge (antenna effect) and at the polymer/air interface. For a 40-μm-thick polymer layer, the electric field intensity increases at a lower rate in the area below polymer deposition compared to the significant and abrupt increase of the electric field intensity at the polymer/air interface and the plate edge. A similar result is shown for 60- and 100-μm-thick polymer layers. However, in all cases the electric field decays exponentially with increasing distance from the plate edge.

When the polymer layer thickness exceeds the height of the plate edges, the electric field first weakens as the antenna effect subsides, then increases suddenly due to the transition from polymer to air dielectric medium, and finally exhibits a decreasing trend with increasing distance from the needle tip. The same behavior is observed in all simulations for a polymer layer extending beyond the plate edges (i.e., polymer layer thickness >100 μm), with a higher electric field intensity arising at the polymer/air interface due to the abrupt change in permittivity. In all cases, the electric field intensity demonstrates a similar exponential decay with increasing distance from the polymer layer, asymptotically approaching the curve corresponding to air dielectric, including the cases of polymer layer thickness of less than 100 μm. This result shows a localized polymer effect on the electric field, i.e., the polymer does not affect the electric field in the air medium (Fig. 1d (inset) and 2b).

Fig. 3 provides further insight into the electric field directionality and intensity at the collector plates. The electric field direction is perpendicular to the plate walls and intensifies in the vicinities of the plate edges. This behavior was observed in all simulations, including the case of air dielectric (Fig. 3a), and indicates that fiber alignment between the plates is due to dipole moments aligned in the direction of the electric field. The results for a polymer layer thickness of 60 μm (Fig. 3b) and 100 μm (Fig. 3c) indicate that the electric field intensity decreases as the polymer thickens due to the strengthening of the dielectric effect. The weakening of the electric field perpendicular to the plate walls caused by polymer thickening is consistent with the experimentally observed progressive diminution of fiber alignment between the plates. However, because the simultaneous fiber deposition between and at the top of the plates may further decrease the electric field intensity, the thickness of the polymer layer with aligned fibers is limited to ~50 μm, in agreement with the experiments performed with the particular mandrel configuration [6,7].

4. Conclusions

An electrostatic FEA analysis of the electrospinning process for a parallel-plate collector was performed to elucidate the fabrication of polymeric bilayer constructs with aligned and randomly oriented fibers. Simulations revealed that the electric field directionality controls the fiber alignment between the plates, and that the decrease of the electric field intensity and loss of directionality with increasing polymer thickness leads to the deposition of randomly oriented fibers. The electrospun polymer produces a local electric effect, instigating significant changes in the electric field intensity in the vicinity of the polymer and an asymptotic approach of the electric field to that for air dielectric. The present analysis can be extended to study other collector configurations, guiding the design of electrospinning systems capable of producing fibrous constructs with various morphologies.

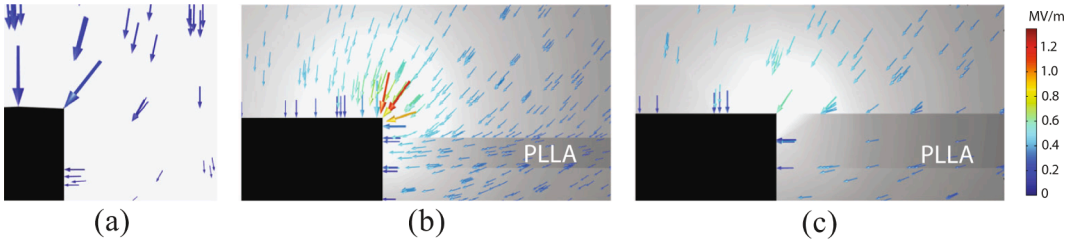

Fig. 3. Electric field in the symmetry plane of the electrospinning setup defined by the mandrel axis and the needle axis for a polymer layer thickness (a) 0 (air), (b) 60, and (c) 100 μm. The vector scaling factor, geometry scale, and color legend of the electric field intensity in (b) and (c) are the same. Only the left plate is shown in each panel. The color of the vectors in (a) is not representative of their magnitudes; it only shows the directionality of the electric field.

Declaration of Competing Interest

The authors declare that they have no known competing financial interests or personal relationships that could have appeared to influence the work reported in this paper.

Acknowledgement

The COMSOL simulation was performed at the Molecular Graphics and Computation Facility, University of California, Berkeley, funded by the National Institute of Health under Grant No. S10OD023532.

References

[1] R.E. Neisiany, et al., Frontiers Mater. 7 (2020) 67.
[2] M. Rahmati, et al., Prog. Mater. Sci. 117 (2021), 100721.
[3] K. Waldrop, R. Wycisk, P.N. Pintauro, Curr. Opin. Electrochem. 21 (2020) 257–264.
[4] M.I. Echeverria Molina, K.G. Malollari, K. Komvopoulos, Frontiers Bioeng, Biotechnol. 9 (2021), 617141.
[5] A. Baji, Y.-W. Mai, S.-C. Wong, M. Abtahi, P. Chen, Compos. Sci. Technol. 70 (2010) 703–718.
[6] J. Pu, F. Yuan, S. Li, K. Komvopoulos, Acta Biomater. 13 (2015) 131–141.
[7] J. Pu, K. Komvopoulos, Acta Biomater. 10 (2014) 2718–2726.
[8] A. Keirouz, M. Chung, J. Kwon, G. Fortunato, N. Radacsi, WIREs Nanomed. Nanobiotechnol. 12 (2020), e1626.
[9] H. Samadian, H. Mobasheri, S. Hasanpour, R. Faridi Majidi, Nanomed. Res. J. 2 (2017) 87–92.
[10] S. Xie, Y. Zeng, Ind. Eng. Chem. Res. 51 (2012) 5336–5345.
[11] E. Huber, et al., IEEE Int. Conf. Electro Inf. Technol. (2016) 788–792.